

Galactic halo cusp-core: tidal compression in mergers

Avishai Dekel, Jonathan Devor & Guy Hetzroni

Racah Institute of Physics, The Hebrew University, Jerusalem 91904, Israel

8 November 2018

ABSTRACT

We explain in simple terms how the buildup of dark haloes by merging compact satellites, as in the CDM cosmology, inevitably leads to an inner cusp of density profile $\rho \propto r^{-\alpha}$ with $\alpha \gtrsim 1$, as seen in cosmological N-body simulations. A flatter halo core with $\alpha < 1$ exerts on the satellites tidal compression in all directions, which prevents deposit of stripped satellite material in the core region. This makes the satellite orbits decay from the radius where $\alpha \sim 1$ to the halo centre with no local tidal mass transfer and thus causes a rapid steepening of the inner profile to $\alpha > 1$. These tidal effects, the resultant steepening of the profile to a cusp, and the stability of this cusp to tandem mergers with compact satellites, are demonstrated using N-body simulations. The transition at $\alpha \sim 1$ is then addressed using toy models in the limiting cases of impulse and adiabatic approximations and using tidal radii for satellites on radial and circular orbits. In an associated paper we address the subsequent slow convergence from either side to an asymptotic stable cusp with $\alpha \gtrsim 1$. Our analysis thus implies that an inner cusp is enforced when small haloes are typically more compact than larger haloes, as in the CDM scenario, such that enough satellite material makes it intact into the inner halo and is deposited there. We conclude that a necessary condition for maintaining a flat core, as indicated by observations, is that the inner regions of the CDM satellite haloes be puffed up by about 50% such that when they merge into a bigger halo they would be disrupted outside the halo core. This puffing up could be due to baryonic feedback processes in small haloes, which may be stimulated by the tidal compression in the halo cores.

Key words: cosmology: theory — dark matter — galaxies: formation — galaxies: haloes — galaxies: interactions — galaxies: structure

1 INTRODUCTION

Cosmological N-body simulations of dissipationless hierarchical clustering from Gaussian initial fluctuations reveal a relatively robust universal shape for the density profile of dark-matter haloes,

$$\rho(r) = \rho_s \left(\frac{r}{r_s} \right)^{-\alpha_0} \left(1 + \frac{r}{r_s} \right)^{\alpha_0 - 3}, \quad (1)$$

where r_s is a characteristic inner radius and ρ_s a corresponding inner density.¹ It has an inner “cusp” $\propto r^{-\alpha_0}$, a turn-over near r_s , and an outer envelope of r^{-3} (or perhaps somewhat steeper) extending out to the virial radius R_v .² Navarro, Frenk & White (1995; 1996; 1997, hereafter NFW) found

eq. (1) with $\alpha_0 \simeq 1$ to be a good fit to haloes in simulations over the radius range $(0.01 - 1)R_v$, for a wide range of halo masses and for a range of hierarchical cosmological scenarios with different power spectra of initial fluctuations. Cole & Lacey (1996) came to a similar conclusion for self-similar scenarios with power-law power spectra, $P_k \propto k^n$ with $n = 0, -1, -2$, in an Einstein-deSitter cosmology. High-resolution simulations of a few individual haloes in a cosmological environment (Moore *et al.* 1998; Ghigna *et al.* 2000; Klypin *et al.* 2001) found that the typical asymptotic cusp profile at $r \ll r_s$ is sometimes somewhat steeper, closer to $\alpha_0 \simeq 1.5$. A careful convergence analysis by Power *et al.* (2002), who explored the robustness to numerical errors, found for the standard Λ CDM cosmology that α_0 reaches a slope shallower than 1.2 at their innermost resolved point of $r \sim 0.005R_v$. Given these uncertainties regarding the exact slope and its extent, the simulations have established the formation of a cusp with a characteristic slope in the range $1 \leq \alpha_0 \leq 1.5$. However, a basic theoretical understanding of its origin is still lacking.

¹ a useful generalized functional form has been proposed by Zhao (1996)

² The virial radius is defined by a fixed mean overdensity Δ_v above the universal mean, with $\Delta_v = 180$ to 340, depending on time and the cosmological model.

An even more intriguing puzzle is introduced by observations of low surface-brightness (LSB) or dwarf galaxies, whose centres are dominated by their dark matter haloes, which indicate that at least in some cases their actual inner halo density profiles are close to flat cores, with $\alpha_0 \simeq 0$ (e.g., van den Bosch *et al.* 2000; de Block *et al.* 2001; Marchesini *et al.* 2002). Similar cores may be present in other galaxies (Salucci & Burkert 2000; Salucci 2001; Borriello & Salucci 2001). This seems to introduce a severe challenge to the CDM cosmological paradigm. Attempts to turn a cusp into a core by direct stellar feedback effects in the present large haloes, which looked promising at a first sight (Navarro, Eke & Frenk 1996), seem not to work in a straightforward way (e.g., Geyer & Burkert 2001; Gnedin & Zhao 2002).

In order to make progress in resolving the core problem, we find it useful to first try to understand in simple basic terms the origin of the universal cusp in the gravitational N-body simulations of cold dark matter. This should provide us with a tool for addressing the formation and survival of flat cores by some non-gravitational mechanism, perhaps by baryonic feedback processes still within the hierarchical CDM framework.

We now return to the issue of dark-halo profiles in dissipationless simulations. The outer slope of r^{-3} (and steeper) may possibly be explained in terms of violent relaxation (e.g., Barnes & Hernquist 1991; Pearce, Thomas & Couchman 1993 and references therein). In general, any finite system would tend to have a steep density fall off at large radii due to diffusion of particles outwards. Secondary spherical infall is expected to produce a profile closer to the profile of an isothermal sphere, $\rho \propto r^{-2}$, which may explain the behavior in the intermediate regions of the halo, but is too steep to explain the flatter inner cusp of $\alpha \leq 1.5$ (Lokas & Hoffman 2000 and references therein). Thus, none of the above mechanisms provides a natural explanation for the characteristic cusp of $\alpha_0 \gtrsim 1$.

By following the evolution in cosmological N-body simulations of hierarchical clustering scenarios, we know that haloes are largely built up by a sequence of mergers of smaller haloes (e.g., Klypin *et al.* 1999b; Moore *et al.* 1999a; Springel *et al.* 2001).³ In a typical merger, a bound satellite halo spirals into the centre of the larger halo due to gravity and dynamical friction. The satellite gradually transfers mass into the host halo due to tidal stripping or by eventually melting into the halo inner region. This process is likely to have an important effect in shaping up the density profile. Indeed, Syer & White (1998), Nusser & Sheth (1999) and Subramanian, Cen & Ostriker (2000) argued, using certain simple models and simulations of a sequence of mergers, that the buildup by mergers may naturally lead to a stable profile. However, they find their predicted profile to be quite sensitive to the power spectrum of fluctuations and to allow an inner slope of $\alpha_0 < 1$, in conflict with the robust result of

³ Although claims were made that a substantial fraction of the mass may actually be added by smooth accretion rather than by mergers, a careful inspection of high resolution CDM simulations shows that this is a wrong impression arising from difficulties in identifying the merging clumps in many cases (e.g., Wechsler, Dekel *et al.*, in preparation).

the cosmological simulations. In fact, when trying to repeat the Syer & White analysis using their simplified modeling of the stripping process but with higher resolution, we find that in the long run the profile does not really converge to a stable cusp but rather continues to steepen slowly towards $\alpha_0 = 3$. Either way, it seems that something is not adequate in the simplified model adopted to describe the mass transfer from the satellite to the halo in these studies.

We re-visit here the buildup of halo profile by merging satellites and gain an encouraging new insight. We add two important new ingredients to the tidal effects. In the current paper, we argue that for a flat mean halo density profile with a logarithmic slope $\alpha \leq 1$ the tidal effects on typical satellites induce three-dimensional compression with no local mass deposit, which results in a rapid steepening of the inner profile to $\alpha > 1$. In an associated paper (Dekel *et al.* 2003) we derive a useful prescription for tidal mass transfer at $\alpha > 1$, and obtain higher deposit efficiency at higher α . We then show that this tends to flatten steep profiles with large α and thus slowly leads to an asymptotic fixed point at a certain $\alpha = \alpha_a \gtrsim 1$.

The key idea in the current paper is that the local tidal mass transfer from the merging satellite to the host halo practically stops when the satellite's orbit has decayed into a core region where the local logarithmic slope is flat, $\alpha(r) \leq 1$. As a result, the satellite continues to sink in due to dynamical friction without mass loss until it settles in the halo centre. This inevitably causes a general steepening of the core profile towards $\alpha > 1$, thus explaining the asymptotic inner slope of the cusp in the NFW profile as seen in the cosmological simulations. We demonstrate this behavior using merger N-body simulations and interpret it using crude analytic approximations in idealized cases.

In §2 we address the α dependence of the tidal force and highlight the three-dimensional tidal compression in a core of $\alpha < 1$. In §3 we describe the N-body merger simulations. In §4 we analyze the evolution of halo density profile in these simulations, where the small satellite is more compact than the more massive halo, as in a typical hierarchical clustering scenario (e.g. Λ CDM). In §5 we qualitatively evaluate the transition in mass-transfer efficiency at $\alpha \sim 1$ in the extreme limits of impulse and adiabatic tidal effects along typical satellite orbits. In §6 we continue to study the α dependence of the mass transfer using the tidal radii for mergers on radial and circular orbits. In §7 we summarize the analysis leading from either side to an asymptotic cusp $\alpha \rightarrow \alpha_a \gtrsim 1$. In §8 we demonstrate how the change from a core to a cusp could be avoided when the merging satellites are slightly puffed up, and discuss a possible scenario for puffing up small haloes by baryonic feedback, perhaps assisted by tidal compression. In §9 we discuss our results and put them in a broader perspective.

2 TIDAL FORCE: COMPRESSION AND STRETCHING

A straightforward analysis indicates that the tidal forces exerted by a dark halo on a satellite orbiting in it depend not

Figure 1. An illustration of the tidal acceleration at a given satellite shell of radius $\ell \ll r$, for a given $\bar{\rho}(r)$ and for different values of halo density-profile slope α [eq. (5) or eq. (6)]. Along the line connecting the centres of mass ($\hat{\boldsymbol{\ell}}_1 = \hat{\mathbf{r}}$) the tides stretch outwards for $\alpha > 1$ and compress inwards for $\alpha < 1$. Along the perpendicular directions, $\boldsymbol{\ell}_2$ or $\boldsymbol{\ell}_3$, there is always compression, independent of α .

only on the distance from the halo centre and the halo mass within that radius, but also on the local slope of the halo density profile. This dependence, which is often overlooked, affects the way mass is transferred from the satellite to the halo, and may provide a clue for the origin of the characteristic cusp of $\alpha \geq 1$ in haloes.

We consider a spherical halo of mass profile $M(r)$ and virial mass M_v . The *mean* density in a sphere of radius r is $\bar{\rho}(r) \propto M(r)/r^3$. A useful quantity in describing the tidal forces exerted by this halo is its local logarithmic slope,

$$\alpha(r) \equiv -\frac{d \ln \bar{\rho}}{d \ln r}, \quad (2)$$

such that locally $\bar{\rho} \propto r^{-\alpha}$. We assume that α is either constant or monotonically increasing as a function of r , with values in the range $0 \leq \alpha \leq 3$. The extreme values of $\alpha = 0$ and 3 correspond to a constant-density halo and a point mass respectively. Note that if the profile inside r is a power law, then the local and mean density profiles have the same logarithmic slope. In general, they are related via $\rho(r) = [1 - \alpha(r)/3]\bar{\rho}(r)$, but they do not necessarily have the same slope at a given r . The slope of $\rho(r)$ is equal to or larger than the slope of $\bar{\rho}(r)$ at any r . The following analysis refers to α as the slope of $\bar{\rho}(r)$.

In the analytic part of our analysis we assume that the density profile of the original halo mass is fixed in time throughout the duration of the merger while the mass torn from the satellite is gradually being added to the halo. This is confirmed to be a reasonable approximation in our N-body merger simulations, where the mass ratio is 1:10 (e.g. Fig. 2).

We then consider a satellite of mass $m_v \ll M_v$, moving under the gravity and dynamical friction exerted by the halo, when the satellite's centre of mass is at position \mathbf{r} as measured from the halo centre. The tidal acceleration exerted by the halo mass distribution on a satellite particle at position vector $\boldsymbol{\ell}$ relative to the satellite centre of mass is obtained by transforming the gravitational attraction exerted by the halo on the particle into the accelerated (non-

rotating)⁴ rest frame of the satellite, namely, by subtracting the acceleration of the satellite centre of mass relative to the halo,

$$\mathbf{F}_t = -\frac{GM(|\mathbf{r} + \boldsymbol{\ell}|)(\mathbf{r} + \boldsymbol{\ell})}{|\mathbf{r} + \boldsymbol{\ell}|^3} + \frac{GM(r)\mathbf{r}}{r^3}. \quad (3)$$

In the tidal limit $\ell \ll r$, this yields to first order in ℓ/r

$$\mathbf{F}_t = \frac{G\ell}{r^3} \left([3M(r) - M'(r)r](\hat{\mathbf{r}} \cdot \hat{\boldsymbol{\ell}})\hat{\mathbf{r}} - M(r)\boldsymbol{\ell} \right), \quad (4)$$

where $M'(r) \equiv dM/dr$. This expression can be simplified using the definition of $\alpha(r)$, which gives $M'(r)r = [3 - \alpha(r)]M(r)$. Using Cartesian coordinates about the satellite centre, where $\boldsymbol{\ell} = (\ell_1, \ell_2, \ell_3)$ and $\boldsymbol{\ell}_1$ lies along \mathbf{r} , we get

$$\mathbf{F}_t = \frac{GM(r)}{r^3} ([\alpha(r) - 1]\boldsymbol{\ell}_1 - \boldsymbol{\ell}_2 - \boldsymbol{\ell}_3). \quad (5)$$

Alternatively, moving to polar coordinates, where θ is the angle between $\boldsymbol{\ell}$ and \mathbf{r} and $\hat{\mathbf{r}} = \cos \theta \hat{\boldsymbol{\ell}} - \sin \theta \hat{\boldsymbol{\theta}}$, we obtain

$$\mathbf{F}_t = \frac{GM(r)\ell}{r^3} \left([\alpha(r) \cos^2 \theta - 1]\hat{\boldsymbol{\ell}} - \alpha(r) \sin \theta \cos \theta \hat{\boldsymbol{\theta}} \right). \quad (6)$$

Fig. 1 illustrates the tidal acceleration at a given satellite shell of radius ℓ in a plane that includes the position vector \mathbf{r} connecting the centres of mass, for given r and $M(r)$ and for different slopes $\alpha = 3, 2, 1$ and 0 . The tidal components along $\boldsymbol{\ell}_2$ and $\boldsymbol{\ell}_3$, perpendicular to \mathbf{r} , are always negative, namely, they exert compression, and they do not explicitly depend on α . Stretching outwards may occur only along $\pm \mathbf{r}$. Unlike the common notion of tidal forces as pulling outwards, the average force on a sphere of radius ℓ is actually inwards: $\langle \mathbf{F}_t \rangle = (GM/r^3)(\alpha/3 - 1)\boldsymbol{\ell}$. It vanishes for a point-mass perturber, $\alpha = 3$, and it obtains a maximum amplitude in a core where $\alpha = 0$.

According to eq. (6), the maximum radial tidal force outwards (towards $+\hat{\boldsymbol{\ell}}$) is always obtained along the line connecting the centres of mass, $\pm \mathbf{r}$. According to eq. (5),

⁴ in some cases it is useful to perform the analysis in a rotating frame, see §6

and as illustrated in Fig. 1, the pull outwards is maximal in the limit where the tides are exerted by a point-mass halo, $\alpha = 3$, valid in the outer regions of typical haloes. For flatter halo profile slopes, the tidal stretching becomes weaker in proportion to $(\alpha - 1)$, until it vanishes at $\alpha = 1$ and reverses direction into compression for $\alpha < 1$. This direction reversal of the tides is often overlooked, because the common context of tides is a perturbation by a concentrated mass distribution. It is a simple result of the fact that the amplitude of the gravitational attraction by the halo, $GM(r)/r^2$, is not a decreasing function of r where the halo mass profile is rising rapidly enough (faster than $M \propto r^2$). Thus, while for $\alpha > 1$ there is always a tidal component pulling outwards, for $\alpha < 1$ the tidal forces are of compression for any θ , namely everywhere in the satellite. In the limit of a constant-density core, $\alpha = 0$, the tides induce symmetric compression in all three dimensions.

We note that the critical slope of $\alpha = 1$ is the asymptotic inner slope of the cusp in the NFW profile. We suggest that this is not a coincidence. The key idea is that if the local tidal mass transfer from the satellite to the halo stops when the satellite's orbit has decayed into a core region where $\alpha(r) \leq 1$, the satellite would continue to sink in due to dynamical friction until it settles in the halo centre. This would inevitably cause a general steepening of the core profile towards $\alpha > 1$. For this scenario to be valid one should verify that, indeed, there is only little local tidal transfer of mass from the satellite to the halo in a region where $\alpha \leq 1$. We first demonstrate this using N-body simulations, and then apply crude analytic approximations in simple cases in order to gain better qualitative understanding of this effect.

3 MERGER SIMULATIONS

For the purpose of investigating the proposed scenario, we run and analyze N-body simulations of isolated mergers between a large halo and a satellite halo of mass ratio $m/M = 0.1$, and then try to interpret them using analytic toy models. We use the Tree code by Mihos & Hernquist (1996 and references therein) with dark-matter haloes only (no gaseous disks). In our default suit of simulations, the large host halo is represented by $N = 10^5$ equal-mass particles and the satellite by $n = 10^4$ particles. We test the sensitivity of our results to resolution by repeating one case with $N + n = 0.55 \times 10^6$ particles and a correspondingly higher force resolution. The simulation units were chosen quite arbitrarily to be: length 3.5kpc, mass $5.6 \times 10^{10} M_\odot$, and time 13.06Myr. The force softening length in the default case is 0.08 units, i.e. 0.28kpc. The units can be properly scaled up or down according to desire. In most cases we refer hereafter to distances and masses in the simulation units, but to time in Myr.

The initial halo density profile, as measured in the unperturbed initial conditions, is a truncated isothermal sphere with a flat core,

$$\rho(r) = \frac{\rho_s e^{-(r/r_t)^2}}{1 + (r/r_s)^2}, \quad (7)$$

Figure 2. The halo profile in the simulation represented by the logarithmic slope α of the mean density profile as a function of radius r (in units of 3.5kpc). Shown are the halo profile at the initial time (solid) and the profiles of the original halo mass at the final times of the radial (long dash) and circular (short dash) merger simulations.

with $\rho_s = 10.36$, $r_s = 1$ and $r_t = 10$. The density at the characteristic radius r_s is thus $\rho(r_s) = 5.13$. The internal velocities are constructed to fulfill the isotropic Jeans equation which ensures an equilibrium configuration as discussed in Mihos & Hernquist (1996). When run in isolation, the halo profile has been tested to be very stable for many dynamical times. As shown in Fig. 2, the logarithmic slope of the density profile spans the range of interest between $\alpha = 0$ and 3, and its variation as a function of radius can be described to a good approximation by $\alpha(r) \approx 1.73 \log r + 0.67$ throughout the range $0.3 \leq \alpha \leq 2.9$. The initial halo density profile will be shown in Fig. 5 below in comparison with the post-merger profile. It resembles the generalized NFW profile of eq. (1) with a core of $\alpha \ll 1$.

The satellite initial density profile is fit by a Hernquist profile,

$$\sigma(\ell) = \frac{\sigma_s}{(\ell/\ell_s) [1 + (\ell/\ell_s)]^3}, \quad (8)$$

with the default choice $\sigma_s = 19.2$ and $\ell_s = 1$ defining our typical “compact” satellite. The initial satellite density profile can also be seen in Fig. 5 below. In the inner region it converges to the NFW profile, $\alpha = 1$. If we fit this Hernquist profile with an NFW profile by matching the characteristic radii where the local logarithmic slope is -2 , we find that the radius corresponding to the characteristic radius of the NFW profile is $\ell = \ell_s/2$. At this radius the density is $16\sigma_s/27$, which for our default satellite is $\sigma(\ell_s/2) = 11.38$.

The satellite parameters were chosen to roughly mimic a typical compact satellite according to the distribution of halo properties in the Λ CDM scenario. In a hierarchical clustering scenario with a fluctuation power spectrum $P_k \propto k^n$, the halo characteristic radii and densities scale like $\ell_s/r_s \propto m^{(1+\nu)/3}$ and $\sigma_s/\rho_s \propto m^{-\nu}$, with $\nu = (3+n)/2$. For Λ CDM on galactic scales one has $\nu \simeq 0.33$. This is

Figure 3. The 10^4 satellite particles in 6 snapshots during the radial (left), circular (right) and elongated (bottom) mergers, projected onto the orbital plane. The 10^5 live halo particles are not shown. The centre of mass is at the origin and the dot marks the temporary halo maximum density. The circle is of radius $r = 20 \simeq 2r_t$ about the halo maximum density, corresponding to where the initial halo practically ends and where the satellite is at the onset of the simulation. The three thirds of the mass, in concentric shells about the satellite bound centre at each time, are marked by different colors.

confirmed by cosmological simulations (NFW; Bullock *et al.* 2001a), where the typical halo profile is NFW. The haloes of lower masses are thus typically more compact; they tend to have lower characteristic radii and higher corresponding mean densities within these radii (corresponding to higher virial concentration parameters). For CDM haloes of mass ratio $m/M = 1/10$, the typical ratio of characteristic radii and corresponding densities are expected to be roughly 0.4 and 2.1. The corresponding ratios in the initial conditions of our simulations are approximately 0.5 and 2.2, providing a reasonable match. It may also be interesting to note that

the satellite mean density interior to $\ell_s/2$ (or ℓ_s) is about 3.9 (or 1.09) times the halo mean density interior to r_s .

We simulated three cases of initial merger orbits: a radial orbit, a circular orbit, and an elongated orbit with an initial pericentre to apocentre ratio of $r_p/r_a \simeq 1/6$. The unperturbed satellite is put initially at $r = 20$, i.e. at about $2r_t$, where the initial circular period is about 230Myr (or about 17.6 simulation time units). In the circular and radial cases the magnitude of the initial satellite velocity was set to equal the circular velocity of the halo at that radius, namely a bound orbit with an orbital kinetic energy that equals half the absolute value of the total energy. For the elongated or-

Figure 4. Time evolution of the satellite spherical mass profile during the radial merger (left) and the circular merger (right). Shown in the bottom panels are the mean radii of concentric spherical shells about the momentary satellite centre, each encompassing a given fraction of the original satellite mass, as labeled on the right. The top panels show the time evolution of position r of the satellite centre relative to the halo centre (dotted), and the corresponding local slope $\alpha(r)$ (solid). For the radial merger, the times of halo-centre crossing are marked in the bottom panel by vertical lines. For the circular merger, representative values of $\alpha(r)$ along the orbit are marked in the bottom panel. The stripping of a shell can be crudely identified by a rapid increase of its radius. Lack of stripping and slight overall contraction of bound shells is noticed whenever the satellite enters the halo core.

bit the initial tangential velocity was about one half of the circular velocity at $r = 20$, in fact $v/v_c = 0.49$. Each merger has been followed until the satellite's bound core has practically settled at the halo centre. Fig. 3 shows the satellite mass distribution in 6 snapshots during the merger process in the three cases, projected onto (one of) the orbital planes.

The radial-orbit merger has been followed for more than 200Myr (about 15 time units), with equal steps of 1.306Myr (0.1 time units) between output times. The satellite is stretched and stripped along the line connecting the centres of mass and the stripping produces the familiar bridge-and-tail tidal structure. An overall shrinking is seen near the first centre crossing, followed by a three-dimensional re-bounce and significant mass loss about the following apocentre (discussed in §5 below). The stripped material shows a sequence of arc-like caustic structures corresponding to each apocentre, reflecting the initial confinement in phase space. The oscillations of the satellite remnant about the halo centre decay rapidly due to dynamical friction until it becomes confined to the halo core after about 115Myr, and it practically melts into the halo central region after $\sim 130 - 140$ Myr. The final distribution of satellite mass extends quite smoothly about the halo centre in a puffy ellipsoid; it is moderately prolate, with the major axis parallel to the original merger line.

The circular-orbit merger has been followed for 836Myr (64 time units) with 81 output times spaced by 10.45Myr. The satellite gradually spirals inwards due to dynamical fric-

tion. The continuous tidal stripping process in the outer parts is obvious. Particles escape from the satellite in the two directions roughly along the line connecting the centres of mass of halo and satellite, and produce the familiar trailing and leading tidal tails because of the differential rotation in the halo potential. The remaining bound satellite seems to be slightly elongated in a direction not far from the line connecting the centres of mass, crudely reflecting the shape of the Roche lobe (see §6 below). After entering the halo core, at about 380Myr, the dynamical friction weakens and the satellite orbit continues to decay very slowly towards the halo centre. The final distribution of satellite mass extends quite smoothly in an oblate configuration about the halo centre.

In the elongated-orbit merger, the satellite oscillates about the halo centre through a sequence of pericentre and apocentre passages. The shape of the orbit remains roughly constant while it shrinks in scale; when measuring the ratio of pericentre to the following apocentre it is $r_p/r_a \sim 1/3.5$, and when measuring the ratio of pericentre to the preceding apocentre it is $r_p/r_a \sim 1/3.5$, but these ratios remain roughly the same for all detectable pericentres. The oscillations decay due to dynamical friction until the satellite becomes confined to the halo core after ~ 125 Myr and 5 pericentre passages. By the first pericentre, the satellite is already stretched and stripped along its orbit, while it is temporarily shrunk in the perpendicular direction. This is followed by a re-bounce and significant mass loss about the

following apocentre. The visual impression confirms the notion that the particles that are torn away near a pericentre radius continue on orbits that reflect on average the satellite orbit at the time of stripping, while the bound remnant is gradually sinking into smaller radii due to continuing dynamical friction (see §5.1 below). For example, in the snapshots corresponding to the second and third apocentres we clearly see a large amount of stripped satellite material spread about the location of the previous apocentre. We can crudely say, in all the mergers simulated, that mass is stripped near pericentre and is practically “deposited” about the following apocentre radius. This crudely validates a toy-model concept that each satellite shell ℓ is being practically deposited at a certain halo radius r . The final distribution of satellite mass extends quite smoothly about the halo centre in a puffy oblate ellipsoid that looks quite symmetric in the orbital plane.

Fig. 2 displayed earlier also shows the $\alpha(r)$ profiles of the original halo material at the final times after the mergers. The relatively small changes in this profile compared to the changes in the profile of the total halo mass (original halo plus stripped satellite material) indicate that the assumption of a fixed halo to which the satellite mass is being added can serve for a crude toy model.

4 PROFILE BUILDUP IN THE SIMULATIONS

Fig. 4 describes the time evolution of the satellite spherical mass profile during the mergers by showing the mean radii of concentric spherical shells about the satellite maximum-density centre, each encompassing a given fraction of the satellite mass (and not necessarily the same population of particles at different times).

In the circular merger case, to a good approximation, the satellite position r is a monotonically decreasing function of time, and so is $\alpha(r)$, as shown at the top and marked along the time axis of Fig. 4. The stripping moment of each shell is marked by the onset of a steep rise in the corresponding curve. Proceeding from the outside shells inwards, the stripping point of each shell can be identified with a specific halo radius r and a corresponding α , moving down monotonically from $\alpha \sim 3$ to flatter slopes. However, as the stripping point passes beyond the radius where $\alpha \sim 1$ (after ~ 380 Myr), when the satellite is left with less than $\sim 30\%$ of its original mass, the stripping slows down and eventually stops. The 20% and inner shells are never really stripped, while the satellite’s orbit continues to decay very slowly towards the halo centre.

In the radial merger case the satellite oscillates about $r = 0$. It crosses the halo core back and forth a few times while the oscillation amplitude is decaying due to dynamical friction until the bound remnant settles at the halo centre. Center crossings occur near the times 22, 62, 83, 99, 110 Myr and so on. The satellite enters the core region in every oscillation a couple of Myr before it crosses the halo centre. Overall contraction of bound satellite shells seems to start roughly at these times, as indicated by the reversal of the tidal forces near $\alpha = 1$ (§2). Each major contraction is fol-

lowed by a re-bounce as the satellite exits the core towards apocentre in the opposite side, which results in overall expansion and stripping of the outer shells.

After about 90 Myr the satellite orbit becomes confined to inside the region where $\alpha < 1.5$, and after about 107 Myr it is confined to the inner halo where $\alpha < 1$. Once the satellite becomes confined to this halo core, there is no apparent overall shell expansion anymore, indicating that stripping has stopped.

In the elongated merger case (not shown to avoid redundancy), pericentre passages are identified five times, and the behavior is qualitatively similar to the radial merger case. Overall contraction of bound satellite shells seems to start roughly at these times. Each major contraction is followed by a re-bounce as the satellite moves towards apocentre, which results in overall expansion and stripping of the outer shells. Once the satellite becomes confined to the inner halo where $\alpha < 1$, after ~ 125 Myr and 5 apocentres, there is no apparent overall shell expansion anymore, indicating that stripping has stopped.

It is important to note that the halo radius r where $\alpha = 1$ is more than three times larger than the radius ℓ of the satellite’s 20% shell, indicating that the cease of stripping occurs significantly before the centre of the bound satellite remnant coincides with the halo centre.

Fig. 5 addresses the cusp formation straightforwardly by showing the density profile of the halo before and after the merger in the three different cases. For the standard, compact satellite, either on radial, circular or elongated orbit, the figure demonstrates the inevitable steepening of the profile in the core region, starting near the core boundary where $\alpha \simeq 1$. In the case of radial merger, the slight depletion of final density in the region near $\alpha \sim 1$, compared to the slight increment in halo density at larger radii, is consistent with no mass transfer in this region while the orbit of the remaining satellite continues to decay into smaller radii. A similar effect is also seen in the circular case, though it is somewhat weaker. Not surprisingly, the steepening seen at $\alpha \lesssim 1$ in the elongated merger case is not very different from the steepening seen in the two other cases.

In order to evaluate the sensitivity of our results to the resolution of the simulation, we ran a case identical to the merger on an elongated orbit described above, but now with 5 times more particles ($N + n = 0.55 \times 10^6$) and a softening length smaller by a factor of $5^{1/3}$ accordingly. The results are found to be practically identical in all respects, including the decay rate of the satellite radius within the halo, the mass loss from the satellite, and the final halo density profile. The latter is shown in the bottom-right panel of Fig. 5. This indicates that the resolution of our simulations is adequate in the range of radii of relevance, well inside the core/cusp region and down to below $0.2r_s$.

We thus learn that one single merger with a 1:10 compact satellite, typical of the Λ CDM cosmology, is enough for turning a core into a cusp of $\alpha \gtrsim 1$. How stable is this cusp under further mergers with similar satellites? To test this, we performed a series of mergers following each other. The main progenitor halo in each merger is taken to be the

Figure 5. Halo density profile before (solid) and after (dashed) the simulated mergers with a compact satellite. The initial halo core becomes a cusp for all types of merger orbits (specified within each panel). A significant fraction of the satellite settles intact at the halo centre without depositing mass near $\alpha \lesssim 1$, causing the steepening of the core into a cusp. The error bars refer to Poisson errors in the r bins, and they are roughly spaced by the bin size. The thin dotted curves mark for reference the initial satellite profile (lower) and a straightforward sum of the initial profiles of halo and satellite (upper). The bottom-right panel corresponds to the same elongated-orbit merger as in the bottom-left panel, but simulated with 5 times more particles (0.55×10^6) and a softening length smaller by a factor of $5^{1/3}$ accordingly. It demonstrates that our default resolution is adequate.

outcome of the previous merger, except that its total mass is scaled down back to the original halo mass (such that all the density profiles can be directly compared). We achieve this by letting each simulation involve the same numbers of N halo particles and n satellite particles (each of a fixed mass m), where the halo particles are selected at random from the $N + n$ particles of the halo produced in the previous merger. In these tandem mergers we used $N = 20,000$ and $n = 2,000$. The halo profile in the range of interest is found to remain stable for at least several hundred Myr when the halo is run in isolation. The satellite starts with the same profile as the original compact satellite. It is put at the same distance of $r = 20$ as before but in an elongated orbit of a random spatial orientation. The initial satellite velocity is tangential to the line connecting the centres of mass of halo and satellite, with an amplitude in units of the circular velocity at $r = 20$ chosen at random in the range $v/v_c = 0.2 - 0.6$ (compared to the typical case simulated

before, where $v/v_c = 0.49$ led to peri/apocentre ratio of roughly 1:6). Each merger was followed for 325 Myr before the following merger started. The density profiles after each of the first 5 mergers are shown in Fig. 6. We see that the first merger reproduces a cusp very similar to the cusp produced when the merger was simulated with $N = 100,000$ (and with $N = 500,000$), Fig. 5, indicating that even $N = 20,000$ is adequate for crude results in the regime of interest here. We see that inside the initial core radius the cusp is stable at a slope of $\alpha \simeq 1.5$, with no systematic tendency to deviate from the power-law profile resulting already after the first merger. At the radius where $\alpha \gtrsim 1.5$ the profile flattens, and the amplitude becomes lower partly because of the renormalization of the total mass between every two mergers.

We conclude that the NFW inner slope of $\alpha = 1$ is indeed a robust lower bound, as indicated by the reversal of the tidal forces there (§2). Any flatter density core does not survive as long as bound satellites bring enough mass into

5.1 Orbits, stripping and deposit

The validity of each approximation depends on the nature of the orbit of the satellite within the halo. Along a typical orbit, the satellite distance from the halo centre oscillates periodically between the radii of apocentre r_a and pericentre r_p , while their amplitudes gradually decay due to dynamical friction. Ghigna *et al.* (1998) studied the distribution of satellite orbits in a high-resolution N-body simulation of a cluster emerging from a CDM cosmological background (mostly in an extended range where $\alpha \sim 2$). They found that the median ratio r_a/r_p is 6:1, with about 25% of the orbits more eccentric than 10:1, and concluded that radial orbits are common while circular orbits are rare. The expected more rapid tidal disruption of satellites on radial orbits may indicate that the actual initial distribution of orbits tended even more towards radial orbits.

Figure 6. Halo density profile after tandem mergers with compact satellites of mass ratio 1:10 on random elongated orbits. The initial halo profile, with a core, is shown for comparison (solid line). After each merger, the total mass of the halo is scaled down back to the original mass. We see that the cusp which forms in the first merger remains stable under the subsequent mergers.

the inner halo and deposit it near the halo centre. This provides a simple explanation for why the cusp slopes seen in cosmological N-body simulations of CDM models are typically $\alpha > 1$. It implies that the only way which may possibly enable a flatter core is by suppressing the settling of satellites in the core, as demonstrated by simulations with puffy satellites (§8).

Next, we continue our effort to understand the tidal mass transfer seen in the simulations. We build upon the α dependence of the tidal forces discussed in §2, and try to evaluate the resultant mass transfer using simple dynamical considerations and idealized toy models.

5 THE IMPULSE AND ADIABATIC LIMITS

In this section we analyze the tidal mass transfer from satellite to halo by referring to particles in orbits within the satellite. The α dependence of the tidal process in the central regions of a halo can be qualitatively evaluated in two extreme limits. If the tidal forces vary on a time scale shorter than the particle orbital periods within the satellite, then one can use the impulse approximation (Spitzer 1958; Binney & Tremaine 1987, hereafter BT, §7.2) to estimate the energy input into the satellite and the resulting mass loss. If the tidal forces vary on a time scale longer than the orbital periods within the satellite, then one can appeal to adiabatic invariants along the particle orbits (e.g., BT §3.7) in order to estimate the gradual energy change of the satellite particles, the associated structural changes in the satellite, and the escape rate.

Ghigna *et al.* (1998) also demonstrated that the tidal radii of the satellites, ℓ_t , are consistent with being determined near pericentre, under the general resonance condition $\bar{\rho}(r_p) \sim \bar{\sigma}(\ell_t)$, where $\bar{\sigma}(\ell) \propto m(\ell)/\ell^3$ is the mean density profile of the satellite. Particles that escape from the satellite can be assumed, on average, to continue on an orbit about the halo centre with apocentre and pericentre radii “frozen” at their values near the time of escape, suffering no further decay due to dynamical friction. Since a particle spends most of its time near the apocentre of its orbit, we can vaguely say that the escapers are effectively “deposited” in the halo near the apocentre radius valid at the time of escape. This effect is clearly seen in our simulation of the radial and elongated merger orbits, e.g., Fig. 3, where a large cloud of stripped particles is seen left behind at each successive apocentre.

Very eccentric orbits may involve “penetrating” encounters near pericentre, where $r_p < \ell$ for ℓ a characteristic radius of the satellite. In this case the tidal approximation becomes invalid. The tides are weakened when the centre of the perturber lies inside the satellite, until they vanish when the satellite centre coincides with the halo centre. It can be shown that the effect of a fast penetrating encounter is comparable to the effect of an encounter with $r_p \sim \ell$ as computed using the impulse approximation in the tidal limit (BT §7.2.e). In a slow penetrating situation the tidal effects simply weaken gradually as $r \rightarrow 0$.

5.2 The impulse limit

The impulse approximation may be partly valid for satellites on elongated orbits during their first quick pericentre passages. As long as $\alpha > 1$ along the orbit, the tidal force, $F_t \propto \bar{\rho}(r)$, has a peaked maximum at the $\sim r_p$ vicinity of the pericentre, where the satellite spends a small fraction of its orbital period. Since $\bar{\rho}(r_p) \sim \bar{\sigma}(\ell_t)$, and since the typical orbital period is inversely proportional to the square-root of the density, the satellite orbital period is comparable to the internal orbital periods of outer satellite particles. Therefore, the impulse approximation may be partly valid for such particles near their apocentres within the satellite.

In the impulse approximation, each satellite particle is assumed to obtain an instantaneous velocity kick Δv , which

is the integral $\int \mathbf{F}_t dt$ over the short duration of effective tides near pericentre along the satellite orbit. The energy change per unit mass of a particle moving with momentary velocity \mathbf{v} is thus $\Delta E = (1/2)(\mathbf{v} + \Delta\mathbf{v})^2 - (1/2)\mathbf{v}^2$, which consists of linear and quadratic terms in $\Delta\mathbf{v}$, namely

$$\Delta E = \mathbf{v} \cdot \Delta\mathbf{v} + (1/2)(\Delta\mathbf{v})^2. \quad (9)$$

Some particles may be kicked by this impulse to above the escape velocity at their position and become unbound.

If the satellite is spherical and the particle motions outwards and inwards are symmetric, a kick inwards is as effective in feeding energy into the satellite as a kick outwards. The contribution of the linear term to the total energy vanishes by the symmetry of incoming and outgoing particles, but the linear term may have an important contribution for the escapers which come from the high-end tail of the ΔE distribution.

The dominant tidal kick $\Delta\mathbf{v}$ is due to the systematic force towards the satellite centre along the direction perpendicular to the orbital plane, where the tidal force is α -independent and persistently inwards [eq. (5)]. A somewhat smaller kick is obtained when integrating the force component along the position vector of the satellite (\mathbf{r}) at pericentre (it is a net kick inwards if $\alpha < 2$), while the contribution along the position vector at apocentre tends to average out when integrated along the orbit (BT §7.2, eq. 7-54; Gnedin, Hernquist & Ostriker 1999).

If indeed $\bar{\rho}(r_p) \sim \bar{\sigma}(\ell_t)$, then the velocity kick integrated along a path of length $\sim r_p$ near pericentre is comparable to the typical particle velocity, $\Delta v \sim v \sim \bar{\rho}(r_p)^{1/2}\ell_t$. This makes the energy change maximal in the outer satellite regions, with comparable contributions from the linear and quadratic terms. The kick inwards causes a delayed escape, because the escapers need to cross the satellite before departure, and the crossing time is comparable to the orbital period in the halo. Therefore, the actual stripping is expected to occur in the halo near the following apocentre, where the particle is “deposited” anyway (§5.1).

When apocentre is at $\alpha > 1$ but pericentre is already in the $\alpha < 1$ regime, the duration of maximum tides becomes longer and the impulse approximation less valid. Any stripping that still occurs along such an orbit ends up with “deposit” outside the $\alpha < 1$ core.

The shrinkage near pericentre and the following re-bounce and later mass deposit near apocentre are clearly seen in the simulations of the radial and elongated mergers, Fig. 3 and Fig. 4.

Once the satellite orbit becomes confined to the inner halo where $\alpha < 1$, we expect no impulse stripping. If the slope near pericentre is α , the tidal force drops to half its peak magnitude at a distance of $\sim 2^{1/\alpha}r_p$ from pericentre. At $\alpha = 1/2$ this is already $4r_p$, so the tidal force is not much weaker than its pericentre value throughout a large fraction of the orbit. Furthermore, adiabatic compression makes $\bar{\sigma}$ become larger than $\bar{\rho}(r_p)$ (§5.3 below). These two effects make the impulse approximation invalid. The effect of the inwards tidal force accelerating an incoming particle

is roughly balanced by the inwards tidal force of similar magnitude working to decelerate the particle when it is going out. In the limit where $\alpha = 0$, the tidal force is the same in all directions and constant in time, so $\int \mathbf{F}_t dt = 0$ along each particle orbit and there is no net impulse.

We conclude that we expect no impulse tidal mass deposit in the core region where $\alpha < 1$: neither during the early quick core passages nor after the decay of the orbit into the core region. This is consistent with the behavior in the radial and elongated merger simulations.

5.3 The adiabatic limit

The adiabatic invariance of actions, which is formally valid when the internal orbital periods are much shorter than the characteristic time over which the external potential is varying, is known to be crudely applicable even when these time scales are comparable to each other (BT, §3.6, Fig. 3-29). Since $\bar{\rho}(r_p) \sim \bar{\sigma}(\ell_t)$, and since for bound satellite particles along the satellite orbit $\ell \leq \ell_t$ and $r \geq r_p$, The satellite particles inwards of the tidal radius are likely to obey the adiabatic approximation at all times. Once the decayed orbit becomes confined to a central halo region of $\alpha < 1$, where the tidal force varies slowly along the orbit and actually tends to a constant when $\alpha \rightarrow 0$, the adiabatic approximation becomes crudely applicable also for the outer satellite particles. Any adiabatic compression of the satellite would strengthen the applicability of this approximation.

In this case, the tides gradually distort the satellite, and may cause slow mass loss mostly outside a momentary tidal radius. Now tidal forces outwards cause stretching and energy gain which may lead to mass loss, while tidal forces inwards cause contraction, make the satellite more bound and do not lead to stripping.

In order to gain some insight into the α dependence of adiabatic tidal effects we consider the following simple example. We see in eq. (5) that the tidal perturbation in each direction ($i = 1, 3$) mimics the force of a harmonic oscillator about the satellite centre,

$$F_{ti} = -k_{ti}\ell_i, \quad k_{ti} \propto \bar{\rho}(r) [(1 - \alpha), 1, 1], \quad (10)$$

except that the force constant along ℓ_1 is negative for $\alpha > 1$. If we assume as a toy model that the satellite core is a homogeneous sphere with density σ_0 , the orbits under its own self gravity are also three-dimensional harmonic oscillators, with

$$F_{0i} = -k_{0i}\ell_i, \quad k_{0i} \propto \sigma_0. \quad (11)$$

This can be generalized to a homogeneous ellipsoid, with different force constants in the different directions, based on Newton’s third theorem (e.g. BT, §2.3, Table 2-1). The perturbed system is thus a 3-dimensional harmonic oscillator, with force constants $k_i = k_{0i} + k_{ti}$, and corresponding frequencies $w_i^2 = k_i$. If the motion of the satellite within the halo introduces slow variations in the tidal perturbation, and correspondingly in k_i , the particles should conserve adiabatic invariants along their orbits. The case of a radial

satellite orbit within the halo is particularly simple because the principle directions remain stationary. The adiabatic invariant of the harmonic oscillator along each direction is the action integral

$$\int v_i^2 dt \propto w_i L_i^2 \propto -E_i/w_i \simeq \text{const.}, \quad (12)$$

where the integral is over the period of the oscillation, L_i is the amplitude of the oscillation, and E_i is the corresponding energy (e.g, BT, §3.6.b). Thus $\Delta E_i \propto -\Delta \omega_i$, meaning that strengthening (weakening) of the force constant k_i , corresponding to an increase (decrease) in w_i , leads to shrinking (stretching) and negative (positive) energy changes. This implies that escape may be caused only for particles moving roughly along the radial-orbit line ($\pm \ell_1$) and only as long as $k_1 \propto \bar{\rho}(r)[1 - \alpha(r)]$ is decreasing while r is decreasing. When the satellite is decaying within a halo core where $\alpha < 1$ and where the forces are towards the satellite centre in all directions, all the force constants are clearly increasing with decreasing r , so there is systematic shrinking in all directions. The corresponding energy changes are negative for all the particles, implying no stripping.

When the satellite orbit becomes confined to a flat core of $\alpha = 0$ and density ρ_0 , the restoring force is constant and fully spheri-symmetric, $\mathbf{F} \propto -(\rho_0 + \sigma_0)\ell$, independent of the actual orbit of the satellite within the halo core. The satellite is then in its most tightly bound configuration. We may expect the situation not to be very different for small α values in the range $\alpha < 1$, as the deviation from spherical symmetry is limited to one direction, along which the force is still restoring and is getting stronger as r decreases.

The general behavior in the merger simulations is consistent with the behavior in the above toy model. We noticed in Fig. 4 that once the satellite becomes confined to the halo core there is no further overall shell expansion, indicating that stripping has stopped. at $\alpha < 1$ can be qualitatively reproduced in the extreme limiting cases where the impulse or the adiabatic approximations may be crudely valid. This provides some intuitive understanding for why the slope of $\alpha \sim 1$ is a critical value below which mass transfer is inefficient.

6 TIDAL RADIUS

We now turn to a complementary approach, where the satellite is addressed as a spherical “onion” from which the outer layers are gradually peeled off by the tides. The α dependence of a slow stripping process can be estimated by means of the momentary tidal radius. This depends on the nature of the orbit of the satellite within the halo, which dictates, for example, whether the most useful frame of reference for defining the tidal radius should be rotating or not.

A lower bound to the tidal radius is obtained rigorously in the (rare) case of a *circular* orbit. If the circular angular velocity is Ω , the potential is stationary in a frame which co-rotates with the same angular velocity, in which the corresponding fictitious centrifugal force should also be taken

into account. In this case, the Jacobi integral J is conserved along the orbit of each satellite particle (see BT, §3.3 and §7.3). This integral is the energy as measured in this rotating frame including in the effective potential the term corresponding to the centrifugal force, $-(\Omega \times \mathbf{x})^2$. The outermost closed zero-velocity surface of constant J defines a firm closed boundary around the satellite, the Roche lobe, which cannot be crossed by particles from the inside out. Therefore, the distance from the satellite to the Lagrange point, the saddle point of the effective potential, provides a lower bound for the tidal radius. This Lagrange point can be obtained by balancing in the rotating satellite frame the self-gravity of the satellite with the sum of the tidal and centrifugal forces along the line connecting the centres of mass. The self-gravity pull inwards by the satellite mass interior to ℓ is $-[Gm(\ell)/\ell^3]\ell$ and the centrifugal force is of an opposite sign and the same amplitude because of co-rotation [$\Omega^2 \propto M(r)/r^3 = m(\ell)/\ell^3$]. Using the ℓ_1 component of the tidal force from eq. (5) we obtain for the tidal radius when the satellite is on a circular orbit of radius r :

$$\alpha(r) \bar{\rho}(r) = \bar{\sigma}(\ell_t) \quad (13)$$

(compare to BT, eq. 7-84, for the case $\alpha = 3$). In this case the combined effect of the tidal and centrifugal forces along the line connecting the centres of mass is always pointing away from the satellite centre, towards $+\hat{\ell}$. This stretching force becomes weaker as α decreases, but it completely vanishes only at $\alpha = 0$. In the direction perpendicular to the line connecting the centres of mass but still in the merger plane the tidal compression along $-\hat{\ell}$ is exactly balanced by the centrifugal force, independent of r and α . In the direction perpendicular to the merger plane, the centrifugal force is zero so the net force is the usual tidal compression, with no explicit α dependence.

In the other extreme (more realistic) case of a merger on a *radial* orbit, the only forces working on the particle in the satellite (non-rotating) rest frame are the tidal force and the self-gravity pull inwards. The direction of maximum tides is stationary, and only the magnitude of the force varies as a function of r . Even though there is no exact analog of the Jacoby integral in this case, one may still define a tidal radius ℓ_t by the point along the line of maximum tides at which the tidal and self-gravity forces balance each other such that the net force in the satellite frame is zero. The condition replacing eq. (13) for a radial orbit is thus

$$[\alpha(r) - 1] \bar{\rho}(r) = \bar{\sigma}(\ell_t). \quad (14)$$

In the above expressions for the tidal radius, the satellite profile is crudely assumed to be fixed in time for $\ell < \ell_t$ and its mass distribution is assumed to remain spherical; the shells outside the tidal radius are assumed to be peeled like layers off an onion while the tidal distortions are neglected.

We now investigate the evolution of the tidal radius, starting with the radial-orbit case. As r is decreasing from the virial radius inwards, where α is large, the function $[\alpha(r) - 1] \bar{\rho}(r)$ is increasing. Assuming that $\bar{\sigma}(\ell)$ is a monotonically decreasing function, this means that ℓ_t is decreasing. More and more mass of the satellite is being torn away as the satellite is moving in. However, as the satellite ap-

proaches the position where α approaches unity, the function $[\alpha(r) - 1]\bar{\rho}(r)$ approaches zero, implying that the tidal radius grows to infinity. This means that there is a halo radius r_m and a corresponding slope $\alpha_m > 1$ at which $[\alpha(r) - 1]\bar{\rho}(r)$ obtains a maximum. If the inner satellite density is high enough, then eq. (14) implies that $\bar{\sigma}(\ell_t)$ obtains a maximum value $\bar{\sigma}_m$ at r_m , and therefore ℓ_t obtains a minimum value ℓ_{tm} there. Since at $r < r_m$ (and $\alpha < \alpha_m$) the tidal radius derived by eq. (14) is larger than ℓ_{tm} , we expect no further stripping inwards of r_m . The slope α_m thus characterizes the point of minimum tidal radius inside which the stripping stops, and ℓ_{tm} marks the boundary of the central part of the satellite which remains intact, not to be disrupted.

The subsequent sinking in of this whole remnant to the halo centre due to dynamical friction causes a steepening of the profile at $r < r_m$ where $\alpha < \alpha_m$. This steepening is effective at least as long as the inner slope is flatter than $\alpha = 1$. It can be avoided only if the inner satellite density is low enough such that $\ell_t = 0$ already at $r > r_m$, namely the satellite is fully disrupted outside the halo core region (see §8 and Fig. 10).

As an example, assume that the *mean* halo density profile is given by eq. (1) with $\rho_s = r_s = 1$, namely $\bar{\rho}(r) = r^{-\alpha_0}(1+r)^{\alpha_0-3}$, and allow the inner slope α_0 to take a value between 0 and 3.⁵ The corresponding α profile is $\alpha(r) = (\alpha_0+3r)/(1+r)$ and we find that $[\alpha(r) - 1]\bar{\rho}(r)$ obtains a maximum at $r_m = (1-\alpha_0)/2 + (3\alpha_0^2 - 12\alpha_0 + 9)^{1/2}/6$. Fig. 7 shows, for a range of α_0 values, the corresponding values of the minimum-tidal-radius quantities r_m , α_m , and the corresponding $\bar{\sigma}(\ell_t)$ according to eq. (14). We see that for a flat core, $\alpha_0 = 0$, the minimum tidal radius is obtained at $\alpha_m = 1.5$ and $r_m = 1$. For larger α_0 in the range $(0, 1)$, the value of α_m gradually decreases towards $\alpha_m = 1$, namely it converges to the asymptotic value $\alpha_0 = 1$ at $r \rightarrow 0$. For $\alpha_0 \geq 1$, the minimum tidal radius is obtained at $r_m = 0$, with $\alpha_m = \alpha_0$. For α_0 in this range the stripping continues until the tidal radius shrinks to zero and the whole satellite is disrupted.

An overall tidal compression at $\alpha < 1$ should actually enhance the steepening effect. It would compactify the satellite while in the halo core and add halo mass to it, which would make the dynamical friction more effective and speed up the orbit decay to the halo centre. Moreover, the halo would react to the addition of satellite mass to its centre by further contraction, preferentially at smaller radii, roughly obeying the adiabatic invariant that requires $Mr \sim \text{const.}$ inside each shell of material.

In the case of a circular orbit, eq. (13), an analogous analysis to the one summarized in Fig. 7, for the example of a mean halo profile given by eq. (1), yields for a core of $\alpha_0 = 0$ a minimum tidal radius at $\alpha_m = 3/4$ (the analog of $\alpha_m = 1.5$ in the radial case). The minimum tidal radius becomes zero and $\alpha_m = \alpha_0$ for any $\alpha_0 > 3/13$ (the analog of $\alpha_0 > 1$ in the radial case). Since eq. (13) provides a lower bound to the tidal radius, these values of α_m should be regarded as lower bounds for the circular-orbit case.

⁵ The corresponding local density profile is a Hernquist profile, $\rho(r) = (1 - \alpha_0/3)r^{-\alpha_0}(1+r)^{\alpha_0-4}$.

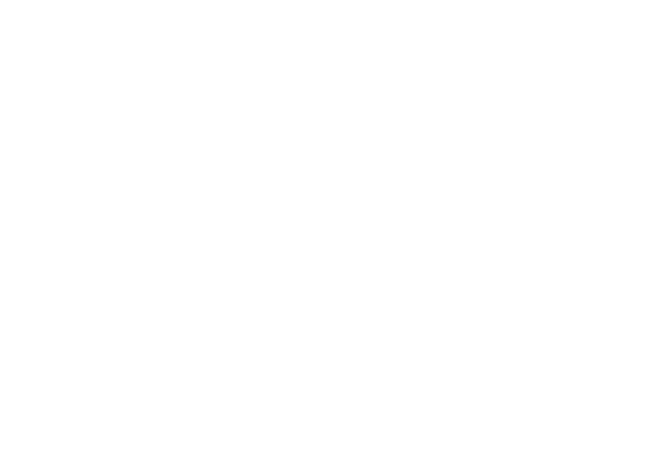


Figure 7. Quantities when the tidal radius obtains a minimum, as a function of the halo inner slope α_0 in eq. (1). Shown are the position in the halo r_m/r_s , the slope α_m and the mean density within the minimum tidal radius $\bar{\sigma}_m(\ell_t)$. Note that $\alpha_m \geq 1$.

Since at a given position in a given halo central region (given α) the stripping seems to be more efficient for satellites on circular orbits than on radial orbits, and the compression is correspondingly less effective, the dynamical friction becomes weaker for circular orbits. This should slow down the dynamical-friction decay of the orbit to the halo centre and the steepening process, as noticed in our N-body simulations.

Thus, based on the current simplified analysis, the satellites on circular orbits are not necessarily as effective as those on radial orbits in steepening cores to cusps. However, we argue in Dekel *et al.* (2003) (as summarized in §7 below) that the α dependence of the mass-transfer efficiency is enough to cause steepening of the profile even by satellites on circular orbits, as is demonstrated by the simulations (§4).

The tidal radius of a satellite on a realistic, elongated orbit is likely to lie in between the radii obeying eq. (14) and eq. (13). At large r (compared to pericentre), an elongated orbit can be approximated as a radial orbit. Near pericentre of an orbit about a point-mass halo the orbit might have resembled a circular orbit, but in a flat halo core the orbit near pericentre is better approximated by a straight line. Thus, the steepening effects of typical satellites on the inner halo profile are more likely to be similar to the effects evaluated for radial orbits. Furthermore, the fact that even in the simulation of a merger on a circular orbit the mass deposit seems to practically stop near $\alpha \sim 1$, not far from the behavior in the radial-orbit case, indicates that the estimate of tidal radius based on the Jacoby integral may indeed be an underestimate.

We conclude that the general behavior in the simulations of tidal mass transfer as a function of $\alpha(r)$ can be qualitatively understood also in terms of the idealized concept of stripping outside a tidal radius.

7 CONVERGENCE TO AN ASYMPTOTIC CUSP

The tidal mass transfer in halo regions where the slope is $\alpha > 1$, and the actual convergence from either side to an asymptotic cusp, are analyzed in an associated paper (Dekel *et al.* 2003). We provide a quick preview of this analysis here for the completeness of the discussion.

We develop a simple prescription for tidal mass transfer by relating every shell ℓ in the initial satellite with a “deposit” radius r in the halo. This is done by equating the encompassed mass within ℓ in the initial satellite with the mass of stripped satellite material found inside halo radius r after the merger, $m(\ell) = m_{\text{fin}}(r)$. This correspondence can be expressed in terms of α :

$$\frac{\bar{\rho}(r)}{\bar{\sigma}(\ell)} = \psi[\alpha(r)], \quad (15)$$

where $\bar{\rho}(r)$ and $\bar{\sigma}(\ell)$ are as before the initial mean density profiles of the halo and the satellite. What makes this prescription useful is that $\psi(\alpha)$ is found to be quite insensitive to the specific nature of the merger (see below). Several authors (e.g., Syer & White 1998; Klypin 1999a) applied the crude resonance condition $\psi = 1$. However, the α dependence of the tidal force, and in particular its vanishing at low α , imply that $\psi(\alpha)$ should be a monotonically *decreasing* function of α . When we adopt the approximation of peeling layers off a fixed onion as above, we obtain from eq. (14) and eq. (13) that $\psi \propto (\alpha - 1)^{-1}$ and $\propto \alpha^{-1}$ respectively. When we also take into account the deposit at apocentre due to stripping at pericentre and the stretching and distortion of the inner satellite mass before it is being torn away⁶, we expect ψ to be smaller than unity even near $\alpha \sim 1$ and to decline further with α at $\alpha > 1$.

We then measure $\ell(r)$ and obtain $\psi(\alpha)$ in several different merger simulations like the ones described above. The measured $\psi(\alpha)$ is found to be qualitatively similar for the different merger cases, despite the very different orbits and initial density contrasts between satellite and halo. [This similarity can be seen from the resemblance of the final profiles $r(\ell)$ in Fig. 4]. An approximate empirical fit is obtained, for example, by $\psi(\alpha) = 0.5/\alpha$, with a spread of less than ± 0.1 about it in the different cases studied. The robustness of $\psi(\alpha)$ indicates that eq. (15) can serve as a useful approximate recipe for tidal mass transfer in the general case. We conclude that the simplified resonance condition, $\psi = 1$, does not provide a good approximation for where the satellite mass ends up. The actual mass transfer is more efficient ($\psi < 0.5$), and its relative efficiency gets higher in steeper regions of the halo profile.

If the mass transfer is described by eq. (15) with $\psi(\alpha)$ declining rapidly enough, we show in Dekel *et al.* (2003) that the profile evolves slowly towards an asymptotic stable power law with $\alpha_a \gtrsim 1$. We assume that the halo and satellite are drawn from a cosmological distribution (as predicted theoretically and seen in simulations); they are ho-

⁶ a decrease in satellite density before stripping has been seen in simulations (e.g. Klypin *et al.* 1999a, Fig. 6; Hayashi *et al.* 2002)

Figure 8. A schematic illustration of satellite mass deposit in the halo. Shown are an NFW halo profile $\bar{\rho}(r)$, and a homologous satellite $\bar{\sigma}(\ell)$ properly shifted to the left and upwards. The arrows connect shell radii ℓ to the halo radii where they are deposited r . The horizontal dashed arrows refer to stripping when stretching is ignored, $\psi(\alpha) = 1$. This would steepen the profile, as steep regions of $\bar{\sigma}(\ell)$ are deposited at flatter regions of $\bar{\rho}(r)$. The solid arrows illustrate realistic stripping after stretching. The vertical displacements, which grow with r , refer to $\psi(\alpha) < 1$. The slope at ℓ may be flatter than the slope at r such that the mass tends to be deposited at larger r and the result is flattening of the halo profile.

mologous, with their characteristic radii and densities scaling like $\ell_s/r_s \propto m^{(1+\nu)/3}$ and $\sigma_s/\rho_s \propto m^{-\nu}$, where $\nu \simeq 0.33$ for Λ CDM. Fig. 8 helps understanding intuitively the origin of an asymptotic slope due to the decreasing nature of $\psi(\alpha)$. We write $\bar{\rho}_{\text{final}}(r) = \bar{\rho}(r) + \bar{\sigma}(\ell)\ell^3/r^3$, and obtain for the change of the local slope in a merger

$$\Delta\alpha(r) \propto -\frac{d}{dr} \left(\frac{\bar{\sigma}(\ell)\ell^3}{\bar{\rho}(r)r^3} \right). \quad (16)$$

While every power law is a self-similar solution, $\Delta\alpha(r) = 0$, it is not necessarily a stable one. For example, with $\psi = \text{const.}$ one would have obtained $\Delta\alpha(r) > 0$ everywhere (because ℓ/r is decreasing with r), namely a continuous steepening towards $\alpha = 3$. On the other hand, a realistic mass transfer where ψ is decreasing with r may produce a stable fixed point where $\Delta\alpha = 0$ and the second derivative is negative. A rigorous linear perturbation analysis determines the rate of convergence and yields an equation for the value of the asymptotic slope α_a under a sequence of mergers with the same mass ratio m/M :

$$\Delta\alpha \propto \alpha(\alpha - 3)\psi'(\alpha)/\psi(\alpha) + 3 \ln[(m/M)^{-\nu}\psi(\alpha)] = 0.$$

The solutions for m/M large enough are typically in the range $1 < \alpha_a \leq 1.5$. For a sequence of mergers with a cosmological distribution of mass ratios we obtain an asymptotic slope comparable to the solution of eq. (7) with $m/M \simeq 0.3$.

In order to test the linear analysis, we perform toy simulations of the profile buildup by cosmological mergers, where we implement the mass-transfer recipe, eq. (15), with $\psi(\alpha) = 0.5/\alpha$. Fig. 9 shows the convergence of α at a fixed r to the asymptotic value. The profile actually evolves through

Figure 10. Halo density profile before (solid) and after (dashed) the merger with a puffy satellite, whose density at the characteristic radius has been scaled down by a factor of about 2.5 compared to the compact satellite. Left: the radial merger simulation. Right: the circular merger simulation. Notation is as in Fig. 5. The puffy satellite loses most of its mass in the outer halo, leaving the halo core practically unaffected.

Figure 9. Toy-simulation evolution of slope α at $r = 0.1r_s$ due to a sequence of mergers with mass ratio $m/M = 0.3$. The initial profile is eq. (1) with α_0 either zero or 2. When $\alpha < 1$, the slope steepens rapidly to $\alpha > 1$ within a few mergers and then it converges slowly from either side towards an asymptotic value.

momentary profiles which are more relevant for comparison with real haloes at different times during their buildup process; they resemble in shape the generalized NFW profile, with an inner cusp growing slowly from $\alpha = 1$ to $\alpha = \alpha_a$. We find a weak sensitivity to the cosmological power spectrum of perturbations, partly because of the robust tidal effect driving the slope to $\alpha > 1$, as discussed in the current paper.

8 A FLAT CORE BY PUFFY SATELLITES

Our robust result so far is that a cusp of $\alpha > 1$ develops in dark-matter haloes whenever mergers with compact satellites bring enough bound clumps to reside in the inner parts of haloes. It implies that a necessary condition for maintaining a flat core is preventing bound clumps from settling in the core. This can be achieved within the Λ CDM scenario

only if the cores of satellite haloes were puffed up significantly by processes other than the gravity of the cold dark matter. In this case the satellites would practically disrupt while the apocentre of their orbit is still in the outer halo, and the halo core could remain undamaged.

How much puffing is needed? In order to obtain a first clue, we have performed simulations similar to those described in §3 and §4, except that the compact satellites of CDM have been replaced by more puffy satellites of the same total mass. In the Hernquist profile, eq. (8), where the default compact satellites had $\sigma_s = 19.2$ and $\ell_s = 1$, the parameters of the puffy satellites are now $\sigma'_s = \sigma_s/8$ and $\ell'_s = 2\ell_s$. With this choice, the density at $\ell = 1/2$, the characteristic radius of the original compact satellite, is scaled down by a factor of 2.3, to just below the density of the host halo at its characteristic radius. This corresponds to a reduction by a factor of 2.8 in the mean density interior to $\ell = 1/2$. Fig. 10 shows the effect of such a merger with a puffy satellite on the halo density profile in the case of circular and radial mergers. When the satellite is puffy, we see that almost all the satellite mass is stripped before the satellite orbit decays to the $\alpha \leq 1$ zone, and as a result the halo core is practically unaffected. We learn that a modest reduction in the initial satellite inner density is enough for preventing the cusp formation seen in Fig. 5.

In fact, mergers with puffy satellites is a plausible mechanism for turning a halo cusp into a flat core. A sequence of such mergers, in which the stripped satellite mass is added to the halo outside its inner region, may lead to a continuous increase of density in the outer halo while the inner density remains unchanged, and thus flatten the inner profile. This process is a subject of ongoing work beyond the scope of the present paper; at the moment it is only a sensible speculation. Our solid result so far is limited to the fact that puffing of the satellites is a necessary condition for halo core survival in the CDM scenario.

Could baryonic feedback effects be responsible for the

puffing up of haloes that could help the haloes maintain their cores, or even turn halo cusps into cores? It is known, for example, that the dissipative infall of the baryons into the halo centre causes adiabatic contraction of the inner dark-matter halo. If a significant fraction of the baryons is then blown out of the galaxy with a velocity much higher than the escape velocity (e.g., as observed by Adelberger *et al.* 2002), then the inner halo may expand in response to a configuration more extended than the original configuration before baryonic infall.⁷ It has been estimated that even in the extreme limit of instantaneous blowout of all the gas the effect on the halo is not strong enough for straightforwardly turning a cusp into a core in a final large halo (Geyer & Burkert 2001; Gnedin & Zhao 2002; though Navarro, Eke & Frenk 1996 find a stronger effect). However, this effect is possibly sufficient for the necessary indirect puffing-up of the merging small haloes. Gnedin & Zhao (2002) estimate that direct feedback effects may reduce the central halo densities by a factor of 2 to 6. Based on our simulations with puffed-up satellites, this may be enough by itself to avoid the steepening from a core to a cusp in the framework of the merging scenario. Furthermore, the strength of the effect depends on how deep in the potential well the gaseous disk resides before it is blown away, which is determined by the baryonic spin. The possibility that baryons in the merging satellites have lost angular momentum due to over-cooling before regaining it by feedback (Navarro & Steinmetz 2000 and references therein; Maller & Dekel 2002, see §9 below) allows one to consider lower spin values than measured in today's disk galaxies, and thus obtain stronger effects on the dark matter.

In fact, one can think of special circumstances within the hierarchical buildup scenario that may boost up the feedback effects even further and help maintaining flat cores. We sketch here such a scenario, based on enhanced feedback in merging satellites due to the tidal compression of the baryons. Consider a satellite made of dark-matter and a typical fraction of baryons merging with the halo on a typical eccentric orbit, which takes the satellite through the halo core to an apocentre in the outer halo a few times before it decays to inside the core region (as in our radial and elongated merger simulations). Assume that cooling in the satellite is efficient such that before the satellite passes through the halo core the baryons are already concentrated in the satellite core, making, say, a half-and-half mixture with the dark matter there. In every passage of the satellite through the halo core, where $\alpha < 1$, the tides compress the satellite into high densities (Fig. 4), creating shocks and stimulating an efficient burst of star formation. (The tides may also induce accretion of material including massive stars from the core of the host galaxy onto the satellite). By the time the satellite is turning around in the following apocentre outside the halo core, the massive stars have produced supernova-driven winds which drive much of the gas out of the satellite. The satellite have already lost much of its outer dark-matter envelope at this point and is basically made of the original satellite core plus most of the satellite baryons. If the satellite core loses half its bound mass in this

gas blow-out, and the gas expulsion is instantaneous, then the satellite becomes completely unbound. But even if the expulsion is slow, the adiabatic invariants imply a density drop by a factor of ~ 8 . Thus, the remaining satellite is now much more susceptible to tidal stripping, which could disrupt it completely before it manages to settle in the halo core. This scenario should be investigated in detail before one can consider it viable. At this point it is just an intriguing speculative proposal for enhanced feedback effects, based on the wisdom gained so far regarding the tidal effects, and very crude common wisdom regarding star formation and feedback (e.g. Dekel & Silk 1986).

9 DISCUSSION

The main result of this paper is that tidal compression enforces an inner cusp of slope $\alpha > 1$ in dark-matter haloes which are subject to tandem mergers with relatively compact satellites as in the Λ CDM cosmology. The lower bound of $\alpha \simeq 1$ coincides with the transition from tidal forces outwards (at $\alpha > 1$) to tidal forces inwards (at $\alpha < 1$), resulting in no local mass transfer from the satellite to the halo near its core boundary and therefore steepening of the core into a cusp. This robust effect is one way to explain the halo inner structure as seen in cosmological N-body simulations of the hierarchical clustering scenario. It then helps providing a tool for addressing other processes which may explain the observed flat cores in (at least some) galaxies. More details of the cusp formation are provided in an associated paper (Dekel *et al.* 2003), where we derive a simple prescription for tidal mass transfer between satellite and halo, and use it to show that successive cosmological mergers slowly lead to a stable asymptotic cusp that is only slightly steeper than $\rho \propto r^{-1}$.

The buildup of a cusp by a single merger with a compact satellite, and in particular the dependence of the tidal mass transfer on the slope of the halo density profile, have been demonstrated using controlled N-body simulations of single isolated mergers. The simulations also indicate that the cusp remains stable under successive, similar mergers. We tried to interpret in simple qualitative terms the detected phenomenon of little mass transfer at $\alpha \lesssim 1$, which gives rise to the steepening to a cusp. For this purpose we used several idealized toy-model considerations based on standard approximations, each valid in another limit and all pointing in the same direction. It is evident that these are simplified approximations, and we expect each to be crudely valid at most during part of the time and for limited parts of the satellite. Nevertheless, we recall that these approximations sometime provide useful qualitative estimates even where there is no formal justification for them to be strictly valid. The fact that in these different regimes the different approximations all point to the phenomenon we see in the simulations may be interpreted as a hint for a qualitative understanding of this phenomenon. One should not use these approximations for making accurate quantitative predictions away from their formal range of validity, and our toy-model analysis is not meant to replace a detailed and definitive exploration using exact analytic dynamical techniques, which should be

⁷ Note, for example, that a virial system that instantaneously loses one half of its mass becomes totally unbound.

the target of subsequent work. However, at this point the cosmological N-body simulations do not give us a clue for the actual origin of the cusp, and the exact methods have not provided a satisfactory understanding yet either. Given that, the controlled merger simulations which highlight a specific key effect, and the idealized approximations which provide hints in the same direction, are useful for making progress in the understanding of the phenomenon associated with the merger process, and in particular for putting forward for further investigation a possible mechanism for cusp formation.

Syer & White (1998) (and independently Nusser & Sheth 1999 and Subramanian, Cen & Ostriker 2000) also addressed the profile resulting from mergers. Although they all see the formation of a cusp in many cases, our results show several differences which one should try to understand. Syer & White implemented the more simplified model of tidal stripping at resonance, $\psi = 1$ in our terms, ignoring the α dependence (and in particular the compression at $\alpha < 1$ and the gradual stretching at $\alpha > 1$). According to their algorithm, the steepening or flattening of the profile is determined solely by whether the satellite inner density is higher or lower than that of the halo. They argue that their prescription allows a long-term survival of a relatively flat core of $\alpha < 1$ and it introduces a strong explicit dependence on the power spectrum of fluctuations — both in conflict with the findings in cosmological simulations. For each of several different power spectra they followed a sequence of mergers and saw an apparent convergence to a different self-similar profile. When we substitute the oversimplified recipe $\psi = 1$ in eq. (16), we find that $\Delta\alpha$ is always positive, for any merger and at any r . Indeed, when trying to repeat the Syer & White toy simulations with higher resolution and following more mergers we actually find that the profile does not really converge to a stable cusp but rather continue to steepen slowly towards $\alpha_0 = 3$. Only when using the improved stripping prescription where ψ is decreasing with α do we obtain convergence to a flatter asymptotic profile. Furthermore, the asymptotic profile obtained via the revised stripping recipe is more robust to the cosmological model. This is partly because the effect of tidal compression drives the profile to $\alpha \gtrsim 1$ independently of the fluctuation power spectrum, and because the cosmological dependence of the ultimate asymptotic slope is weakened by the fact that the profile is determined by mergers of relatively large mass ratio (see Dekel *et al.* 2003).

Somewhat puzzling is the finding of power-spectrum dependence in the profile resulting from a sequence of N-body merger simulations by Syer & White, and especially the apparent slope flatter than $\alpha = 1$ found in one of their cases. It is puzzling because these simulations should have automatically included the correct tidal effects. We can only suspect that the main shortcomings of their N-body simulations are the limited resolution within the cusp region (only 8000 particles in the whole halo) and perhaps the fixed narrow range of satellite masses.

The gravitational processes leading to a cusp are modeled in our analysis as tidal effects during the buildup of the halo by a sequence of *mergers*. This picture is likely to be valid in the CDM hierarchical clustering scenario, where

numerous sub-galactic haloes exist on all scales and are continuously merging (e.g., Klypin *et al.* 1999b; Moore *et al.* 1999a; Springel *et al.* 2001). This merger picture is confirmed by a careful inspection of high resolution CDM simulations, where a special effort is made to identify the merging clumps which otherwise could have been easily missed (e.g., Wechsler, Dekel *et al.*, in preparation). It is therefore clear that cores, independently of how they form, cannot survive in a pure CDM scenario without some modification — they efficiently turn into cusps as a result of the mergers with the relatively compact building blocks.

Nevertheless, a cusp, though somewhat flatter, is reported to be seen also in simulations where the initial fluctuations had less power on small scales, thus suppressing the number of sub-galactic satellites and the associated merger rate (Moore *et al.* 1999b; Avila-Reese *et al.* 2001; Bullock, Kravtsov & Colin 2002). Further indications for the generality of cusp formation comes from simulations by Huss, Jain & Steinmetz (1999), who find that cusps also form as a result of collapse from roughly spherical initial density perturbations with random velocity perturbations, as well as from the simulations of Alvarez, Shapiro & Martel (2002), who find that cusps arise from the gravitational instability and fragmentation of cosmological pancakes. One way to explain this is by noticing that the asymptotic cusp formed in the CDM scenario is driven by mergers with relatively massive satellites (of typical mass ratio 1:3, see Dekel *et al.* 2003), and realizing that such mergers do happen even when small-scale power is suppressed and when pancakes fragment. It is therefore possible that the cusp is actually driven by mergers to a certain extent also in these cases. If it turns out that a cusp also forms when the merger picture is strictly invalid, it would imply that the gravitational processes involved in the halo buildup somehow mimic a behavior similar to the merger case. We note in particular that the tidal compression discussed above is expected to amplify density perturbations and possibly make them behave in certain ways like merging satellites.

More generally speaking, however, one should accept the fact the halo buildup is a complex gravitational process, whose different aspects can probably be modeled in more than one way, e.g., as a violent relaxation process driven by fluctuations in comparison with a sequence of mergers and substructure accretion.⁸ There is also the intriguing possibility that general statistical considerations in phase space may provide some clue for the origin of a universal halo profile (e.g., Taylor & Navarro 2001). Unfortunately, we currently know of no viable alternative to the tidal effects in mergers as a simple model for the origin of $\alpha \gtrsim 1$ cusps in the cosmological simulations. The idealized merger picture provides one possible toy model, properly valid at least in hierarchical clustering scenarios, within which the origin of the cusp is understood in simple terms.

Our result implies a *necessary* condition for the survival

⁸ We encounter an analogous duality, for example, when one manages to explain the origin of galactic spin alternatively via tidal torque theory applied to shells and by summing up the orbital angular momenta in a cosmological sequence of mergers (see Maller, Dekel & Somerville 2002).

of cores in haloes independent of their origin — that satellites should be prevented from adding mass to the halo cores. This could be avoided in a CDM scenario if feedback processes manage to puff up the small haloes and make them disrupt before they merge with the halo cores. We have not explicitly addressed in this paper the *sufficient* conditions for the formation of cores, but one can imagine that a sequence of mergers with low-density satellites, where the mass is predominantly deposited outside the inner halo region, would indeed flatten the inner profiles (work in progress).

Supernova feedback effects are probably not strong enough for turning cusps into cores in haloes with rotation velocities higher than $\sim 100 \text{ km s}^{-1}$, but the feedback may be sufficient for lowering the inner densities in the small halo progenitors such that when they merge they give rise to cores. However, if the (so far inconclusive) observational clues for cores in clusters of galaxies are confirmed, simple supernova feedback is unlikely to provide a viable explanation for their origin. In this case one may search for higher efficiency in supernova feedback either due to microscopic effects such as porosity in a multiphase ISM or due to hypernova from very massive stars (Silk 2002). Alternatively, one may appeal to stronger feedback mechanisms, perhaps associated with radio jets from AGNs. This process may be indicated by an observed correlation between AGN activity and bright galaxies in SDSS (Kauffmann *et al.* 2003, in preparation), and it may be needed independently in order to explain the missing baryons in big galaxies (Klypin, Zhao & Somerville 2002) and in clusters. Otherwise, such large cores may present a real challenge for the standard hierarchical clustering scenario.

Other processes may also contribute to the development of halo cores. One proposed scenario is based on scattering of inner halo particles off central, massive black holes (e.g., Merritt & Cruz 2001). This could be useful in explaining the centres of early type galaxies, but one might suspect that it would be difficult to apply this scenario on the scales of $\sim 10 \text{ kpc}$ corresponding to halo cores, which are much larger than the scales associated with the black hole(s). A second scenario addresses the heating of halo particles by gas clouds spiraling in due to dynamical friction (El-Zant, Shlosman & Hoffman 2002). This is based on assumed specific gradients of velocity dispersion in the inner haloes, which may or may not be valid. A third explanation is based on an efficient angular-momentum transfer from a big rotating bar into the halo (Weinberg & Katz 2002). /

However, other simulations indicate that this effect is inefficient (Valenzuela & Klypin 2002). It has been demonstrated (Sellwood 2002) that the Weinberg & Katz result is likely to be an artifact of the unrealistically large bar assumed, and the representation of this bar by a rigid body. We stress again that, no matter what the origin of the core might be, our analysis implies that such cores could survive only if they are not perturbed by significant mass transfer from merging compact satellites, which implies that small CDM haloes must be puffed up before they merge into bigger haloes. We also stress that none of these scenarios seem to be capable of explaining the formation of cores in haloes on the scales of clusters of galaxies within the CDM scenario.

A possible caveat, which could in principle jeopardize

our results as well as the whole current standard paradigm regarding the validity of N-body simulations in demonstrating robust cusp formation, has been raised by Katz & Weinberg (2002). They claim that all current cosmological simulations fail to recover the actual formation of a core in dark-matter haloes because the N-body noise smears out a delicate resonant reaction of halo-core orbits to the tidal perturbation by the satellite. Based on linear analysis and smoothed-potential simulations, they argue that an induced global mode dominates the process and invalidates the standard dynamical friction approximation by Chandrasekhar. As a result, satellites do not decay into the core but are rather disrupted outside it, thus maintaining a flat core profile at small radii. The dominance of this effect in realistic cases has not been conclusively demonstrated. It is hard to imagine how the resonances can remain so isolated and stable in systems where phase mixing and broadening of resonances are expected. The linear analysis is far from being valid in the nonlinear case in hand, and the over-smoothing in their simulations may hide physical gradients that may spread out the resonances (A. Klypin, private communication). Even if this resonant behavior turns out to be important in the $N \rightarrow \infty$ limit, its relevance in real galaxies is questionable, where the baryons are likely to introduce clumpiness at a level comparable to the granularity in current N-body simulations. Still, this is a caveat worth pursuing.

The cusp/core problem is only one of the difficulties facing galaxy formation theory within the CDM cosmology. It turns out that other main problems can also be modeled by tidal effects in mergers, and may also be resolved by the inevitable feedback processes. For example, Maller & Dekel (2002) addressed the angular-momentum problem, where simulations including gas produce disks smaller than the galactic disks observed (Navarro & Steinmetz 2000 and references therein; Governato *et al.* 2002), and with a different internal distribution of angular momentum (Bullock *et al.* 2001b; van den Bosch, Burkert & Swaters 2001). A toy model has been constructed for the angular-momentum buildup by mergers based on tidal stripping and dynamical friction, which helps us understand the origin of the spin problem as a result of over-cooling in satellites. A simple model of feedback has then been incorporated, motivated by Dekel & Silk (1986). This model can remedy the discrepancies, and in particular explain simultaneously the low baryon fraction and angular-momentum profiles in dwarf disk galaxies.

Various feedback effects may also provide the cure to the missing dwarf problem, where the predicted large number of dwarf haloes in CDM can possibly match the observed number of dwarf galaxies only if the mass-to-light ratio in these objects is very high (Klypin *et al.* 1999b; Moore *et al.* 1999a; Springel *et al.* 2001; Kochanek 2001). Bullock, Kravtsov & Weinberg (2000), Somerville (2002) and Tully *et al.* (2002) appeal to radiative feedback effects which prevent the formation of small dwarfs after cosmological reionization at $z \sim 7$, Scappapietra, Ferrara & Broadhurst (2000) and Scappapietra & Broadhurst (2001) address the destructive effect of outflows from one galaxy on neighboring protogalaxies via ram pressure, and Dekel & Woo (2002) study the role of supernova feedback in determining the relevant

global properties of dwarfs and larger low-surface-brightness galaxies. We note that while the requirements from feedback in explaining the dwarf-galaxy properties and the angular-momentum problem are not too demanding, the solution to the core problem requires that the dark-matter distribution be affected by feedback, which is a non-trivial requirement.

Nevertheless, the successes of such toy models in matching several independent observations indicate that they indeed capture the relevant basic elements of the complex processes involved, and in particular that feedback effects may indeed provide the cure to some or all the main problems of galaxy formation theory within the Λ CDM cosmology that does so well on larger scales. The alternative solution involving Warm Dark Matter (e.g., Hogan & Dalcanton 2000; Avila-Reese *et al.* 2001; Bode, Ostriker & Turok 2001) seems to still suffer to some extent from the core problem, it may still fail to reproduce the angular-momentum profile in galaxies (Bullock, Kravtsov & Colin 2002), and it may be an overkill where the formation of dwarf galaxies is totally suppressed once the inevitable feedback effects are included (Bullock 2001). The speculative alternatives involving self-interacting dark matter are even more problematic (Spergel & Steinhardt 2000; Dave *et al.* 2001; Hennawi & Ostriker 2002).

ACKNOWLEDGMENTS

We acknowledge stimulating discussions with Itai Arad, George Blumenthal, Andi Burkert, Doug Lin and Gary Mamon. This research has been supported by the Israel Science Foundation grant 213/02, by the US-Israel Bi-National Science Foundation grant 98-00217, by the German-Israel Science Foundation grant I-629-62.14/1999, and by NASA ATP grant NAG5-8218.

REFERENCES

Adelberger, K.L., Steidel, C.C., Shapley, A.E. & Pettini, M. 2002, ApJ, astro-ph/0210314

Alvarez, M.A., Shapiro, P.R. & Martel, H. 2002, AAS, 200, 4103

Avila-Reese, V., Colmn, P., Valenzuela, O., D'Onghia, E. & Firmani, C. 2001, ApJ, 559, 516

Barnes, J.E. & Hernquist, L. 1991, ApJL, 370, L65.

Binney, J. & Tremaine, S. 1987, *Galactic Dynamics* (Princeton University Press), BT

Bode, P., Ostriker, J.P. & Turok, N. 2001, ApJ, 556, 93

Borriello, A. & Salucci, P. 2001, MNRAS, 323, 285

van den Bosch, F.C., Burkert, A. & Swaters, R.A. 2001, MNRAS, 326, 1205

van den Bosch, F.C., Robertson, B.E., Dalcanton, J.J. & de Blok, W.J.G. 2000, AJ, 119, 1579

Bullock, J.S. 2001, astro-ph/0111005

Bullock, J.S., Dekel, A., Kolatt, T.S., Kravtsov, A.V., Klypin, A.A., Porciani, C. & Primack, J.R. 2001b, ApJ, 555, 240

Bullock, J.S., Kolatt, T.S., Sigad, Y., Somerville, R.S., Kravtsov, A.V., Klypin, A.A., Primack, J.R. & Dekel, A. 2001a, MNRAS, 321, 559

Bullock, J.S., Kravtsov A.V. & Colin P. 2002, ApJL, 564, 1

Bullock J.S., Kravtsov A.V. & Weinberg D.H. 2000, ApJ, 539, 517

Cole, S. & Lacey, C. 1996, MNRAS, 281, 716

Dave, R., Spergel, D.N., Steinhardt, P.J. & Wandelt, B.D. 2001, ApJ, 547, 574

de Blok, W.J.G., McGaugh, S.S., Bosma, A. & Rubin, V.C. 2001, ApJL, 552, L23

Dekel, A., Arad, I., Devor, J. & Birnboim, Y. 2003, ApJ, 588, in press (astro-ph/0205448)

Dekel, A. & Silk J. 1986, ApJ, 303, 39

Dekel, A. & Woo, J. 2002, astro-ph/0210454

El-Zant, A., Shlosman, I. & Hoffman, Y. 2002, astro-ph/0103386

Geyer, M.P. & Burkert, A. 2001, MNRAS, 323, 988

Ghigna, S., Moore, B., Governato, F., Lake, G., Quinn, T. & Stadel, J. 1998, MNRAS, 300, 146

Ghigna, S., Moore, B., Governato, F., Lake, G., Quinn, T. & Stadel, J. 2000, ApJ, 544, 616

Gnedin, O.Y. & Zhao, H. 2002, MNRAS (astro-ph/0108108)

Governato, F., Mayer, L., Wadsley, J., Gardner, J.P., Willman, B., Hayashi, E., Quinn, T., Stadel, J. & Lake, G. 2002, astro-ph/0207044

Hayashi, E., Navarro, J.F., Taylor, J.E., Stadel, J. & Quinn, T. 2002, astro-ph/0203004

Hennawi, J.F. & Ostriker, J.P. 2002, ApJ, 572, 41

Hogan C.J. & Dalcanton J.J. 2000, PRD, 62

Huss, A., Jain, B. & Steinmetz, M. 1999, ApJ, 517, 64

Katz, N. & Weinberg, M.D. 2002, in Cozumel

Klypin, A., Gottlber, S., Kravtsov, A.V. & Khokhlov, A.M. 1999a, ApJ, 516, 530

Klypin, A.A., Kravtsov, A.V., Bullock, J.S. & Primack, J.R. 2001, ApJ, 554, 903

Klypin, A., Kravtsov, A.V., Valenzuela, O. & Prada, F. 1999b, ApJ, 522, 82

Klypin A., Zhao H., Somerville R.S., 2002, ApJ, 573, 597

Kochanek, C.S. 2001, astro-ph/0108160

Lokas, E.L. & Hoffman, Y. 2000, ApJL, 542, L139

Maller A.H. & Dekel A. 2002, MNRAS, 335, 487

Maller A.H., Dekel A. & Somerville, R.S. 2002, MNRAS, 329, 423

Marchesini, D., D'Onghia, E., Chincarini, G., Firmani, C., Conconi, P., Molinari, E. & Zacchei, A. 2002, ApJ, in press (astro-ph/0202075)

Merritt, D & Cruz, F. 2001, ApJL, 551, L41

Mihos, J.C. & Hernquist, L. 1996, ApJ, 464, 641

Moore, B., Ghigna, S., Governato, F., Lake, G., Quinn, T., Stadel, J. & Tozzi, P. 1999a, ApJL, 524, L19

Moore, B., Governato, F., Quinn, T., Stadel, J. & Lake, G. 1998, ApJL, 499, L5

Moore, B., Quinn, T., Governato, F., Stadel, J. & Lake, G. 1999b, MNRAS, 310, 1147

Navarro J.F., Eke, V.R. & Frenk C.S. 1996, MNRAS, 283, L72

Navarro J.F., Frenk C.S. & White S.D.M. 1995, MNRAS, 275, 56

Navarro J.F., Frenk C.S. & White S.D.M. 1996, ApJ, 462, 563

Navarro J.F., Frenk C.S. & White S.D.M. 1997, ApJ, 490, 493

Navarro J.F. & Steinmetz M. 2000, ApJ, 538, 477

Nusser, A. & Sheth, R. 1999, MNRAS, 303, 685

Pearce, F.R., Thomas, P.A. & Couchman, H.M.P. 1993, MNRAS, 286, 865

Power, C., Navarro, J.F., Jenkins, A., Frenk, C.S., White, S.D.M., Springel, V., Stadel, J & Quinn, T. 2002, MNRAS, submitted (astro-ph/0201544)

Salucci, P. 2001, MNRAS, 320, L1

Salucci, P. & Burkert, A. 2000, ApJL, 537, L9

Scappapioco, E. & Broadhurst, T. 2001, ApJ, 549, 28

Scappapioco, E., Ferrara, A. & Broadhurst, T. 2000, ApJL, 536, L11

Sellwood, J.A. 2002, astro-ph/0210079

Silk J., 2002, MNRAS, submitted (astro-ph/0212068)

Somerville, R.S. 2002, ApJL, 572, L23

Spergel, D.N. & Steinhardt, P.J. 2000, PRL, 84, 3760

Springel, V., White, S.D.M., Tormen, G. & Kauffmann, G. 2001, MNRAS, 328, 726

Subramanian, K., Cen, R., & Ostriker, J.P. 2000, ApJ, 538, 528

Syer, D. & White, S.D.M. 1998, MNRAS, 293, 337

Taylor, J.E. & Navarro, J.F. 2001, ApJ, 563, 483

Tully R.B., Somerville R.S., Trentham N., Verheijen, M.A.W., 2002, ApJ, 569, 573

Valenzuela, O. & Klypin, A. 2002, astro-ph/0204028

Weinberg, M.D. & Katz, N. 2002, astro-ph/0110632

Zhao, H. 1996, MNRAS, 278, 488

